
**Title:** Computational study of fingering phenomenon in heavy oil reservoir with water drive

**Authors:** Wijeratne, D. I. E., & Halvorsen, B. M.

**Article citation**: Wijeratne, D. I. E., & Halvorsen, B. M. (2015). Computational study of fingering phenomenon in heavy oil reservoir with water drive. *Fuel, 158*, 306-314. doi: http://dx.doi.org/10.1016/j.fuel.2015.05.052

# Computational study of fingering phenomenon in heavy oil reservoir with water drive

D.I Erandi N. Wijeratne, Britt M. Halvorsen

Telemark University College
Department of Process-, Energy and Environmental Technology
N-3901 Porsgrunn, Norway

**Abstract**

The objective of this paper is to numerically study the flow in heavy oil reservoir with water drive. The main focus is to investigate the fingering phenomenon and how it affects the oil recovery. 2D simulations were carried out using ANSYS as the Computational Fluid Dynamics software. Cross section of a reservoir is simulated to study the fingering behavior; an instability which occurs in the water oil contact (WOC) zone. Fingering occurs due to heterogeneities in the porous media and the interaction of several forces. Velocity and pressure profiles, breakthrough times and flow rates were studied. Furthermore, the critical velocity is calculated to indicate the instable flow region. The very low velocity of the water oil interface is sufficient to create the instabilities of the water front.

The ANSYS VOF model is verified against experimental data for viscous fingering found in literature. Reasonable agreement between the experimental and simulated results was obtained. Simulations were performed to check the grid size and time step size dependency.

Keywords: Fingering phenomena, heavy oil reservoir, water drive, water-oil interface, CFD, multiphase flow

# 1. Introduction

California is one of the largest oil and gas producing states in the world and has large amounts of heavy oil reserves which are left in the reservoirs due to production difficulties. Recovery of heavy viscous oil is a challenging task due to formation of finger-like patterns from the water oil interface which causes early water breakthrough affecting the oil recovery.

Fingering is well-known phenomenon in heavy oil production, particularly in solvent based processes for the recovery of heavy oil which greatly affect the sweep efficiency. The viscous fingering instability has been the subject of study for over thirty years because of the interesting underlying physics and the significance in many areas involving fluid flow through porous media [1].

Fingering generally refers to the onset and evolution of instabilities that occur in the displacement of fluids in porous media [2]. Instabilities occur in both miscible and immiscible displacement processes and originate on the interface between the phases (as between oil and water). This is due to heterogeneities in the porous media as well as the interaction of different forces. The acting forces are viscous forces driven by adverse viscosity ratios, gravity forces due to density differences, capillary forces due to interfacial tension between immiscible fluids and dispersive forces due to concentration gradients between miscible fluids. The effect of the forces can cause an unstable displacement process. In this study the porous media is homogeneous and since the two phases are not miscible, the dispersive forces do not make any impact.

In the process of displacement of heavy oil by the less viscous fluid, water, the viscous forces are dominating. The viscosity ratio is high and unfavorable which causes fingering due to viscous instabilities [3]. The less viscous displacing fluid generally flows more easily than the more viscous displaced fluid, causing the occurrence of perturbations which is fingering through the system. The viscous fingering increases with the viscosity ratio, between the displaced and displacing fluids.

Figure 1 shows the experimental results carried out by Van Meurs [4,5] involving displacement of oil by water for different viscosity ratios. It is clear that at low viscosity ratio (Figure 1a), the oil/water interface is stable and oil is displaced with great efficiency, and hence the recovery at the time of breakthrough is very high. At higher viscosity ratio (Figure 1b), the fingers can be clearly observed and are seen to be mainly parallel to the flow direction. The water/oil interface is unstable and water invasion occurs in the form of fingers. Considerable amount of oil is bypassed as a consequence of this fingering effect. It can be noted that the contours of these fingers are not smooth but exhibit protrusions of water enclosing oil pockets. These protrusions do not advance in the direction of flow [4,5].

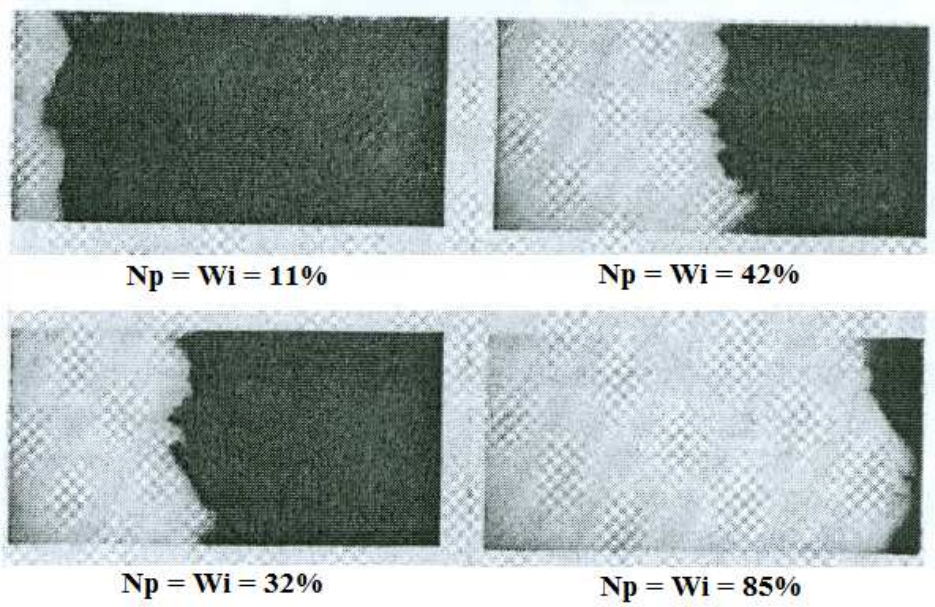


(a)

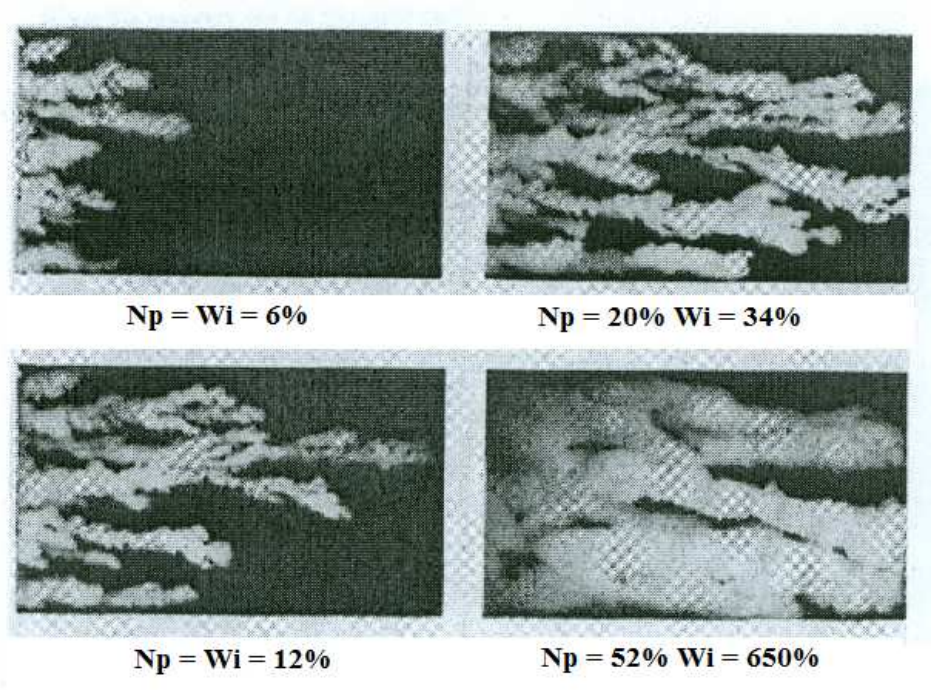


(b)

Figure 1: Linear water drive processes in homogeneous formation [4,5]
(a) $\mu_o/\mu_w = 1$ (b) $\mu_o/\mu_w = 80$

*Np* and *Wi* indicate the progress of flooding, where *Np* is the cumulative oil production in percentage of pore volume and *Wi* is the cumulative amount of water injected in percentage of pore volume.

The development of fingers has been well explained by Homsy (1987) as a process of splitting, shielding and spreading [1]. When the surface tension becomes weak, the front of a steady finger is susceptible to viscous fingering instability by the basic mechanism associated with a less viscous fluid displacing a more viscous one. After a split, each of the new fingers is stable as a result of being thinner than the original finger. Shielding represents the development of a large finger and is affected by flow rate and mobility ratio. As a result of shielding, long fingers suppress the growth of smaller fingers. The smaller fingers will later merge with the large finger and the result is large upswept areas in the reservoir. Spreading arise as a result of the tendency of the fingers to grow due to dispersion. During this process, the finger may reach a width that is unstable and again trigger the splitting and these patterns are repeated [1]. In addition, high speed flow in the finger generates transverse pressure gradients that cause the tips of fingers to be spread, and tail of the fingers to be narrower [2].

Homsy [1] has made following simple argument in order to understand the basic mechanism of the instability when only the gravity and viscous forces are considered. If a displacement in a homogeneous porous medium of constant permeability *K* is considered, the flow involves displacement of a fluid of viscosity $\mu_1$ and density $\rho_1$ by a second fluid of viscosity $\mu_2$ and density $\rho_2$. Under suitable continuum assumption the flow will be assumed to follow Darcy's law, which for a one-dimensional steady flow is expressed by:

$$\frac{dp}{dx} = -\mu U / K + \rho g \tag{1}$$

Considering a sharp interface or zone where density, viscosity and concentration change rapidly, then the pressure force on the displaced fluid as a result of a virtual displacement of *dx* is:

$$dp = \left[(\mu_1 - \mu_2) \cdot \frac{U}{K} + (\rho_2 - \rho_1) \cdot g\right] dx \tag{2}$$

If the net pressure force is positive, then any small displacement will amplify, leading to instability, if not the perturbations will be dampened out. Both gravitational and viscous forces can have either stabilizing or a destabilizing influence depending upon which of the two fluids is denser or more viscous and depending upon the direction and velocity of displacement. The critical velocity $U_C$ above which instabilities occur is:

$$U_C = \frac{(\rho_1 - \rho_2) \cdot gK}{(\mu_1 - \mu_2)} \tag{3}$$

A simpler statement can be made when the gravity force is absent, as in the case of horizontal displacement of oil by water. In this case instability always results when a more viscous fluid is displaced by a less viscous one (in a homogeneous porous media), since the less viscous fluid has the higher mobility. The mobility ratio is defined as [3]:

$$M = \frac{k_{rw} / \mu_w}{k_{ro} / \mu_o} \tag{4}$$

where $k_{rw}$ and $k_{ro}$ are relative permeability for water and oil, and $\mu_w$ and $\mu_o$ are viscosity of water and oil respectively. If $M \leq 1$, the water cannot travel faster than oil, and the oil is displaced in a piston like manner which is the most favorable form of displacement. If $M > 1$, water may channel through oil in an unstable manner and cause the occurrence of frontal instabilities.

The influence of surface tension is not accounted for in the above examples. The interfacial tension may have both a dampening and promoting effect on viscous fingers for unstable immiscible flow. Generally the interfacial tension works to suppress an increase in surface area, but in the case of an already developed finger, interfacial tension will prevent the development of small perturbations on the finger surface. This results in all the fluid flowing into the already developed finger, promoting its growth [3].

Several fundamental, unresolved questions remain. The interface tension due to capillary pressure is determined by the relative ability of the porous medium to be wetted by the displaced or the displacing phase. These wetting effects play a critical role in governing the essential physics. However, it should be noted that there are no possibilities to specify the wetting feature of the two phases in ANSYS/Fluent. The purpose of a stability analysis is to determine the conditions under which small perturbations of the displacement front will grow into viscous fingers. Earlier studies found in literature have reported stability analysis of immiscible displacements covering mobility ratio, capillary and gravitational forces, displacement velocity, and permeability and wettability. However, a combined effect of these parameters is to the authors' knowledge not reported.

# 2. Validation of CFD VOF model

Simulations were carried out using ANSYS/Fluent as the Computational Fluid Dynamics (CFD) software and a model was built up and validated against experimental data found in literature. Volume of Fluid (VOF) is used as the multiphase model. The VOF model can be used to model two or more immiscible fluids by solving a single set of momentum equations and tracking the volume fraction of each of the fluids throughout the domain. The tracking of the interface(s) is accomplished by the solution of a continuity equation for the volume fraction of one (or more) of the phases [6]. Geo-Reconstruct is used as the VOF Scheme. This is the most accurate interface tracking scheme, and is recommended for most transient VOF calculations [6]. The displaced fluid is defined as the primary phase and displacing fluid is defined as the secondary phase. The effect of surface tension along the interface between two phases is included by defining the surface tension coefficient. Porous region is specified with the viscous resistance under cell zone conditions. Since the flow rate through the porous media is very low (laminar flow), Ergun equation can be simplified as below:

$$\frac{\Delta p}{l} \approx \frac{V\mu}{\alpha} \tag{5}$$

The viscous resistance coefficient (1/α) is defined and the inertial resistance (the turbulent component) is set to be zero. The operating pressure is specified. PISO (Pressure Implicit with Splitting of Operators) scheme is used as the Pressure-Velocity Coupling method, the body-force-weighted scheme as pressure discretisation scheme and second order upwind method as momentum discretisation scheme [7].

The model is validated against experimental data found in literature. However, there are only few displacement experiments in literature which use fluids with high viscosity ratio. Experimental models have been used for studying the mechanism of flow processes in oil reservoirs which are scaled for prototypes for large scale studies [4, 8, 9]. In most of these experiments, the displacement velocities were defined whereas the pressure conditions were not defined. Didler Pavone [8] has carried out experiments to observe and characterise viscous fingering patterns in 3D, natural consolidated samples [8]. From the experimental results he was able to correlate parameters like breakthrough recovery, mean local saturation, finger volume and width, pressure drop and saturation profiles with dimensionless numbers. Instabilities were observed by using simple molding technique with epoxy solidification. Two of his experimental cases were selected for simulations in order to verify the ANSYS/Fluent VOF model for further use in this study. The porous sample size was 300 mm in length and 100mm in diameter. The experimental conditions for the two cases are given in Table 1. The details about experimental procedure can be found in the original paper referred to as [8].

*Table 1: Experimental Characteristics of two cases*

| | Case 1 | Case 2 |
|---|---|---|
| Oil (silicon oil) viscosity [cP] | 450 | 150 |
| Resin (epoxy resin) viscosity [cP] | 66 | 66 |
| Viscosity ratio [-] | 6.82 | 2.27 |
| Oil density [kg/m$^3$] | 970 | 970 |
| Resin density [kg/m$^3$] | 1200 | 1200 |
| Porosity [-] | 0.38 | 0.38 |
| Permeability [D] | 1.8 | 0.7 |
| Inlet resin velocity [m/s] | 3.70e-05 | 2.23e-05 |
| Interface tension [mN/m] | 7.5 | 7.5 |
| Operating Pressure [Mpa] | 1 | 1 |

Permeability and oil viscosity of Case 1 correspond to the reservoir conditions used in the reservoir simulations presented in Chapter 3. Three-dimensional simulations were carried out for the two cases presented above. Maximum time step is 3 seconds and the mesh size is 0.003×0.003 m$^2$. The inlet is specified as a velocity inlet boundary and outlet as a pressure outlet boundary. Monitor is set to have pressure drop between the inlet and outlet. The finger formation was observed during the simulation. Figure 2 and 3 show the phase contours of the two cases at the time of breakthrough. Fingering patterns, maximum pressure and breakthrough times obtained in the simulations are compared with the experimental results and presented in Table 2.

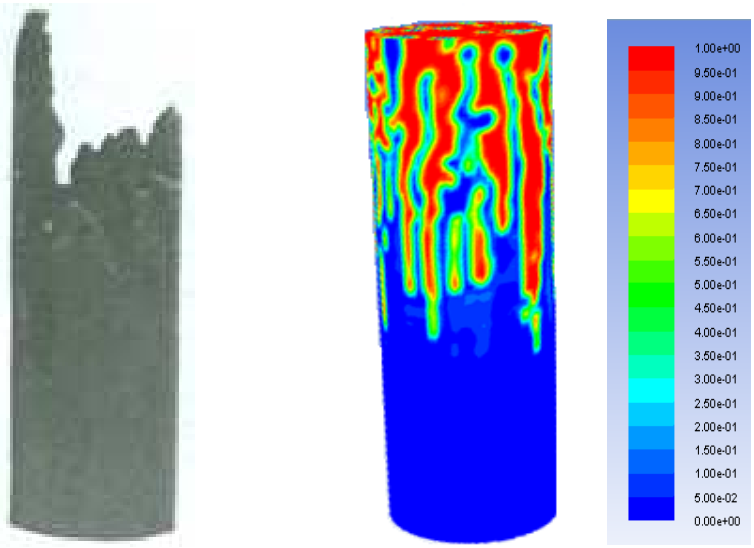


(a) (b)

Figure 2: Phase distribution at breakthrough, contours of volume fraction of the resin. Case 1 (a) Experiment from Didler Pavone [8], (b) Simulation

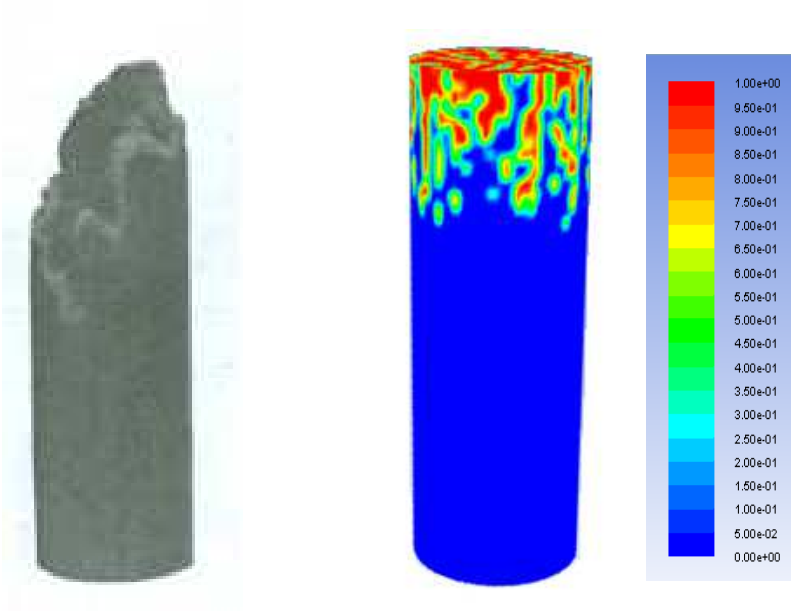


(a) (b)

Figure 3: Phase distribution at breakthrough, contours of volume fraction of the resin. Case 2 (a) Experiment from Didler Pavone [8], (b) Simulation

*Table 2: Comparison of experimental and simulated results for two cases*

| | Case 1 | | Case 2 | |
|---|---|---|---|---|
| | Experiment | Simulation | Experiment | Simulation |
| Number of fingers | 8 | 12-13 | 4-5 | 6-7 |
| Maximum pressure (bar) | 11 | 14 | 6 | 7.2 |
| Breakthrough time (hrs) | 0.7 | 0.54 | 2 | 1.25 |

The finger development as shown in Figure 2 and 3 was observed to have finger branching and coalescence with adjacent fingers. This behaviour results in islands of oil surrounded by the resin. According to the figures there is acceptable qualitative agreement between experimental and simulated results. According to Table 2 the simulation results regarding number of fingers, maximum pressure and breakthrough time are also in good agreement with the experimental values. Based on this, it can be concluded that the ANSYS VOF model used in the further reservoir simulation has been capable of providing reliable results.

# 3. Computational study of fingering phenomenon in heavy oil reservoir

Two-dimensional simulations of the reservoir flow were performed using the validated VOF model. The following assumptions were used; the reservoir field is rectangular with constant thickness and constant pressure boundaries, water drive from the bottom, the reservoir is homogeneous and the initial oil and water saturation is 100% in oil and water layers respectively. The reservoir properties used in the simulation are given in Table 3 and the geometry is presented in Figure 4.

*Table 3: Reservoir and fluid properties*

| | | | |
|---|---|---|---|
| Distance from the wellbore to the oil-water interface [m] | 5.0 | Reservoir pressure [bar] | 30 |
| Water-oil interfacial tension [mN/m] | 25 | Well bore pressure [bar] | 27 |
| Width of drainage area [m] | 10x2 | Water viscosity [cP] | 0.5 |
| Height of oil layer [m] | 10 | Water density [kg/m$^3$] | 1000 |
| Height of water layer [m] | 1.0 | Oil viscosity [cP] | 300 |
| Wellbore diameter [m] | 0.22 | Oil density [kg/m$^3$] | 920 |
| Length of one horizontal section [m] | 12.4 | Rock permeability [D] | 3.0 |
| Rock porosity [-] | 0.3 | | |

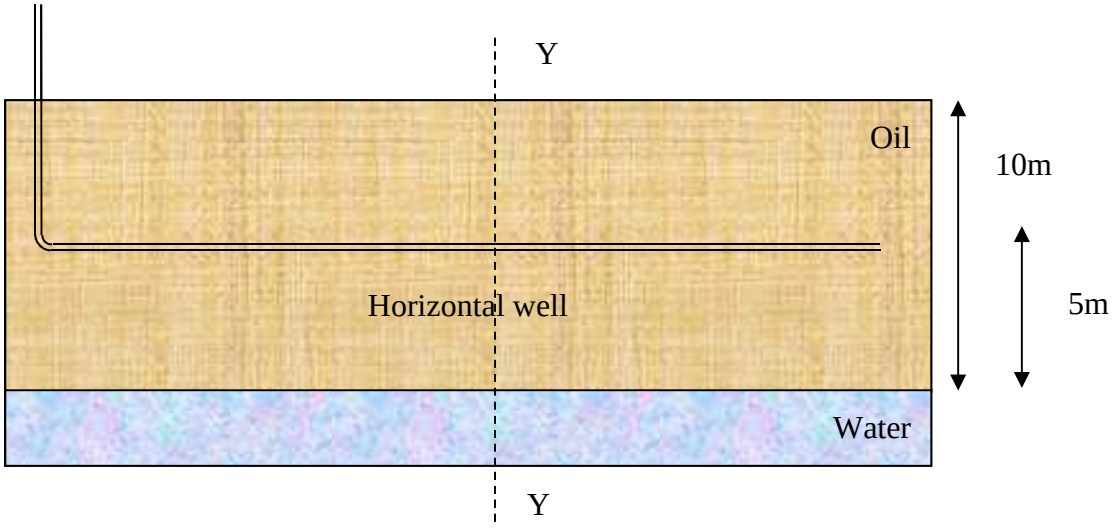


Figure 4: The geometry of the reservoir

To simulate the reservoir flow to the well bore, the cross section (Y-Y) of the reservoir is selected. The cross section view of the reservoir including the boundary conditions is shown in Figure 5.

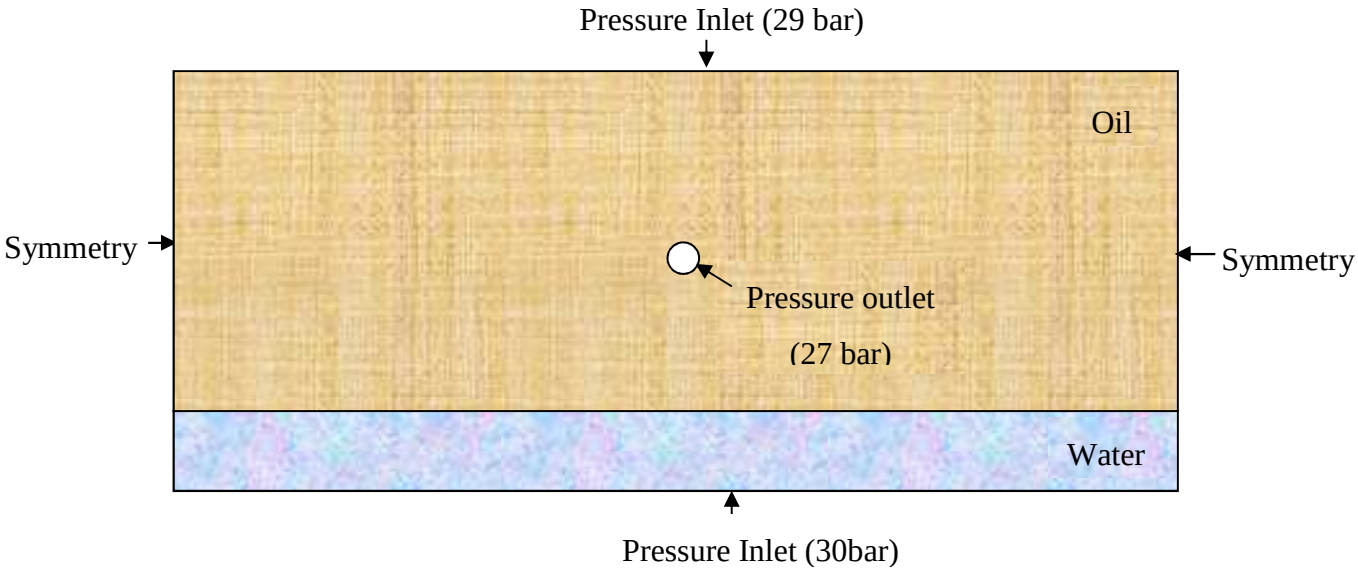


Figure 5: Cross sectional view of the reservoir

The numerical grid for the above geometry is created using GAMBIT. A fine mesh was used near the well bore to capture the small scale structure of the flow in this position. The entire region was meshed using Pave scheme. Grid size dependency simulations were performed and based on the simulations a grid size of 0.06m×0.06m was selected. The total number of cells was 74,000. The total mesh is presented in Figure 6(a), and an enlarged view of the mesh near the well bore is shown in Figure 6(b).

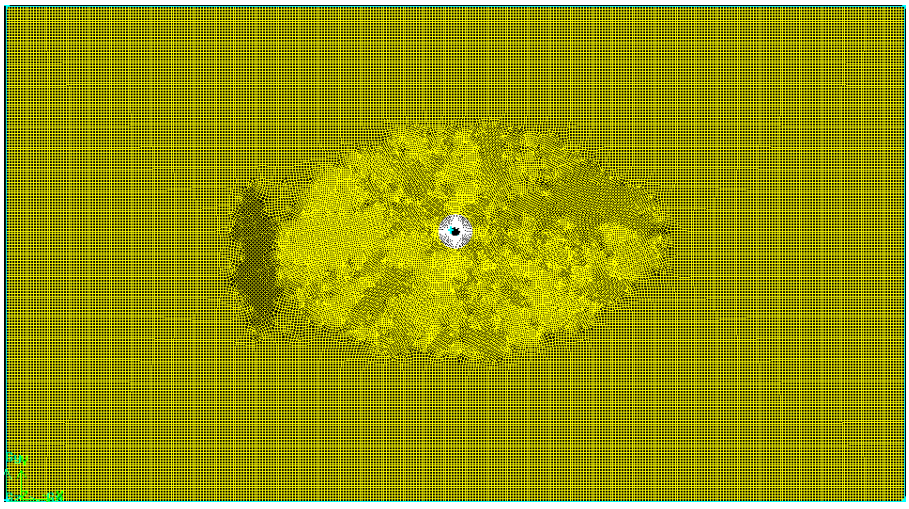

(a)

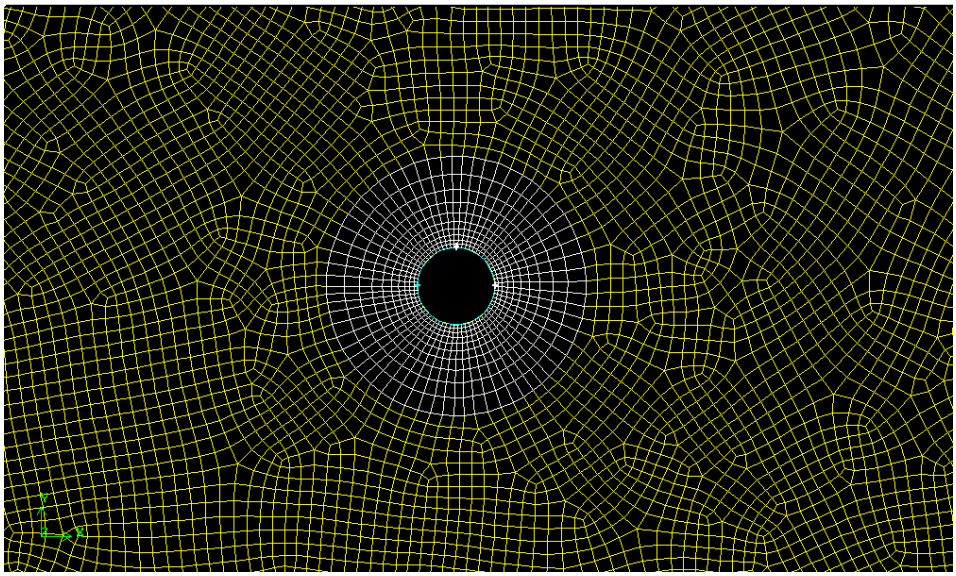

(b)

Figure 6: Reservoir geometry created using GAMBIT. (a) Meshed Geometry. (b) Enlarged view of mesh near the well bore

A two-dimensional, transient, explicit model was developed in ANSYS/Fluent. The boundary conditions are specified in Figure 5. VOF (volume of fluid) is used as the multiphase model in ANSYS/Fluent as described in Chapter 2. The summary of boundary conditions is given in Table 4.

*Table 4: Summary of Boundary Conditions*

| | Boundary Type and value |
|---|---|
| Inlet | Pressure inlet 30 bar<br>Water VF=1 |
| Outlet | Pressure outlet 27 bar |
| Oil | Pressure inlet 29 bar |
| The two ends of the drainage area | Symmetry |

The oil and water layer are marked in order to patch with their respective initial volume fractions. The simulation was carried out for different time steps and 10,000 seconds is selected as the most suitable time step. Numerical instabilities can cause problems after water breakthrough due to very high Courant numbers. The Courant number is defined as $\Delta t / (\Delta x_{cell} / v_{fluid})$.

Fixed time steps were used until water breakthrough and after the breakthrough variable time steps are used and Courant number is set to 70 to allow the simulation to run for a longer time. Monitors are specified to record the flow rates of oil and water. Animations are included

to observe the finger growth as the simulation runs. The initial phase distribution is shown in Figure 7.


Figure 7: Initial Phase Distribution

The same scale for volume fraction of oil is applied to all figures which show phase distribution at different stages of oil production in this paper. Figure 8 shows the phase distribution after 5.8 days of oil production. The oil water interface has started to move towards the wellbore. Figure 9 shows the Static Pressure Distribution after 5.8 days of production. The legend for static pressure is also applied to all figures which show static pressure at different stages of oil production in this study. Figure 10 shows the variation of static pressure along y axis through the well bore after 5.8 days of production.

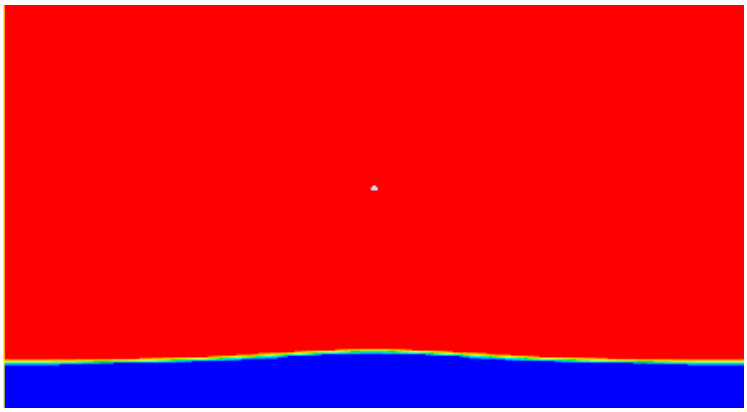

Figure 8: Phase distribution after 5.8 days

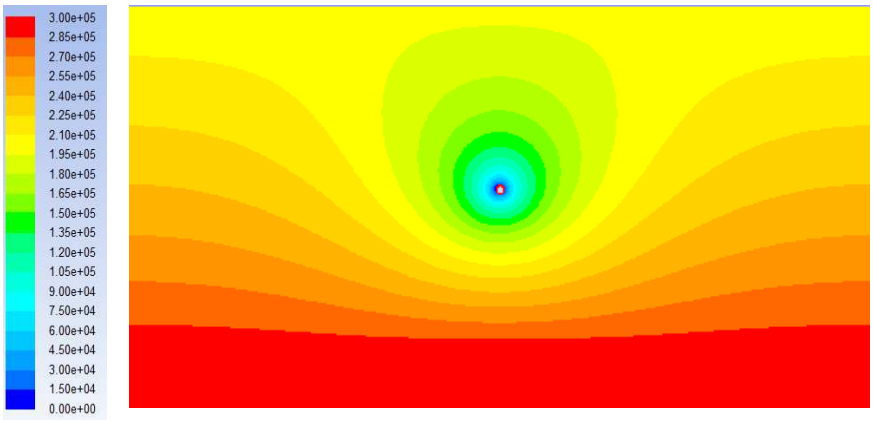


Figure 9: Static pressure distribution after 5.8 days

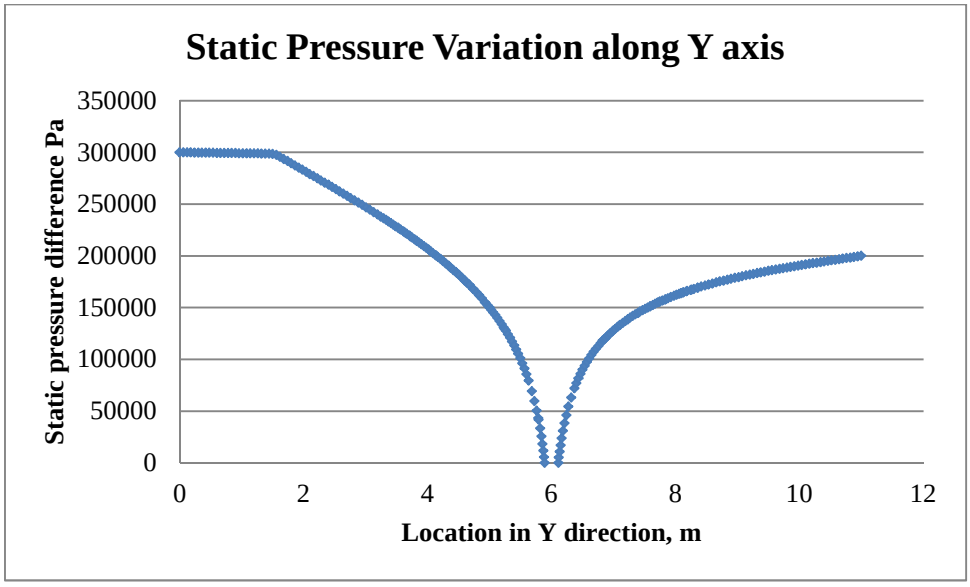


Figure 10: Static Pressure variation along Y direction after 5.8 days.

Figure 11 shows the velocity of the water oil interface after 5.8 days. This corresponds to the shape of the water oil interface shown in Figure 8. The velocity is very low and in the order of $10^{-7}$ m/s which corresponds to displacement velocities representative for oil fields [8]. Maximum velocity, $U_{max}$, is reported at the centre point below the wellbore and is about $3.28 \cdot 10^{-7}$ m/s. The velocity of the interface decreases at location away from the center and the minimum velocity, $U_{min}$ , is about $1.25 \cdot 10^{-7}$ m/s.

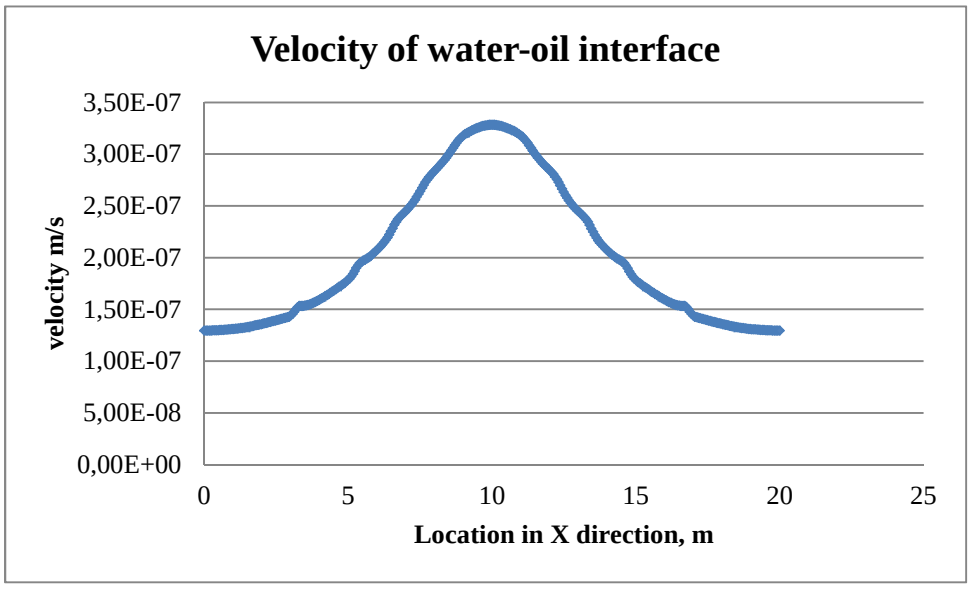


Figure 11: Velocity variation of water-oil interface after 5.8 days

The critical velocity, $U_C$, is calculated based on the following values: $\rho_{water}$ = 1000 kg/m$^3$, $\rho_{oil}$ = 920kg/m$^3$, $g$ = 9.81m/s$^2$, $K$ = 2.96e-12 m$^2$, $\mu_{water}$ = 0.5cP and $\mu_{oil}$ = 300cP. The critical velocity is: $U_C = 7.75 \cdot 10^{-9}$m/s (upwards). Since $U_{max}$ and $U_{min}$ are much higher than $U_c$, flow instabilities occur and finger like pattern starts to appear at the interface. Figure 12 shows the fingering behaviour during oil production.

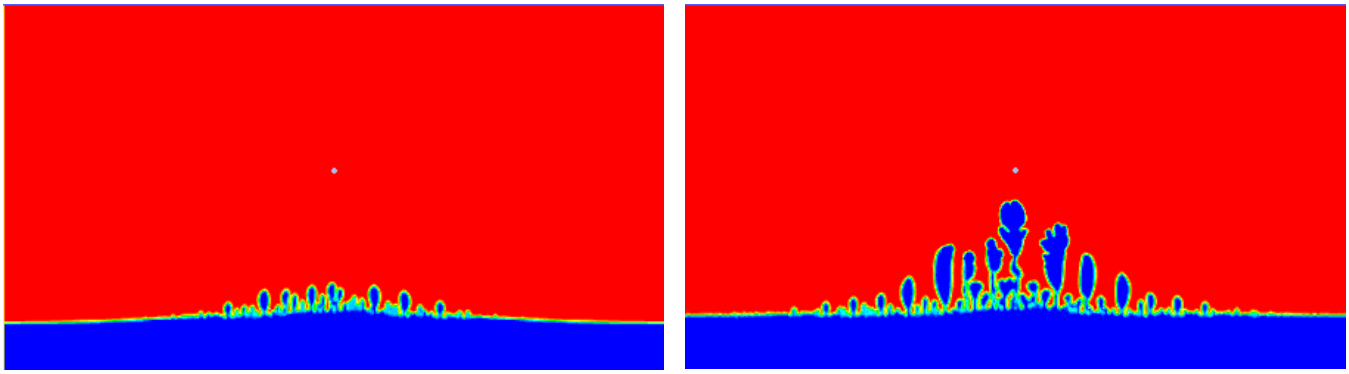

(a) (b)

Figure 12: Phase distribution (a) after 11.6 days and (b) after 17.4 days

The finger pattern and pressure variation at the time of water breakthrough to the wellbore are presented in Figure 13. Breakthrough occurs after 18 days of production. The resulting fingering pattern of the simulation exhibits some interesting characteristics. The tip of the finger has grown wider while the tail has become narrower. The tip is split and tends to form new fingers. The breakthrough occurs from the longest finger which is formed in the center.

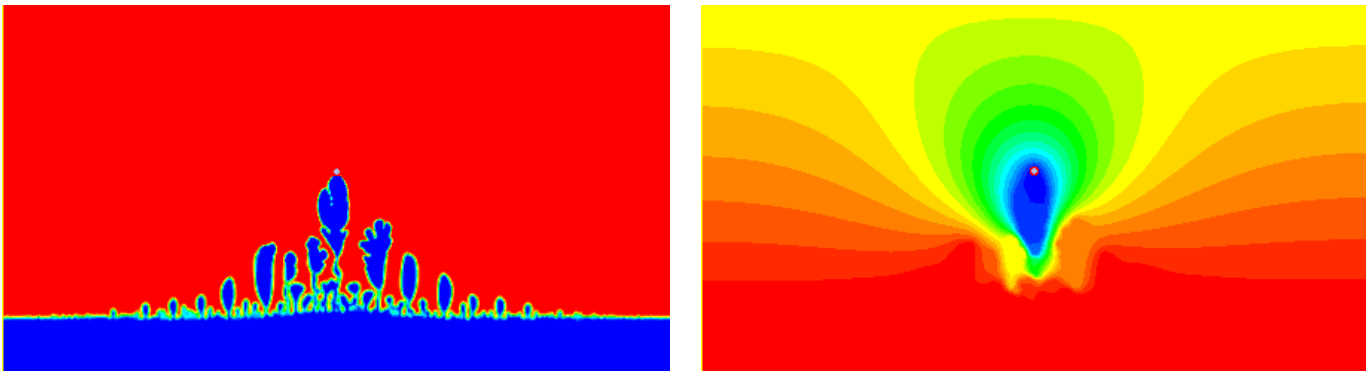

(a) (b)

Figure 13: (a) Phase distribution and (b) Static pressure distribution (blue is the lowest pressure) at the breakthrough, 18 days

Figure 14 gives the static pressure variation at different times of oil production until breakthrough. According to Figure 9 and 13(b) the inlet pressure is propagating towards the wellbore as the finger development takes place. At the time of breakthrough the finger attains approximately the pressure of the wellbore. Therefore there is a considerable pressure drop between the narrowest point of the finger (tail) and free surface as shown in the Figure 14 (blue line).

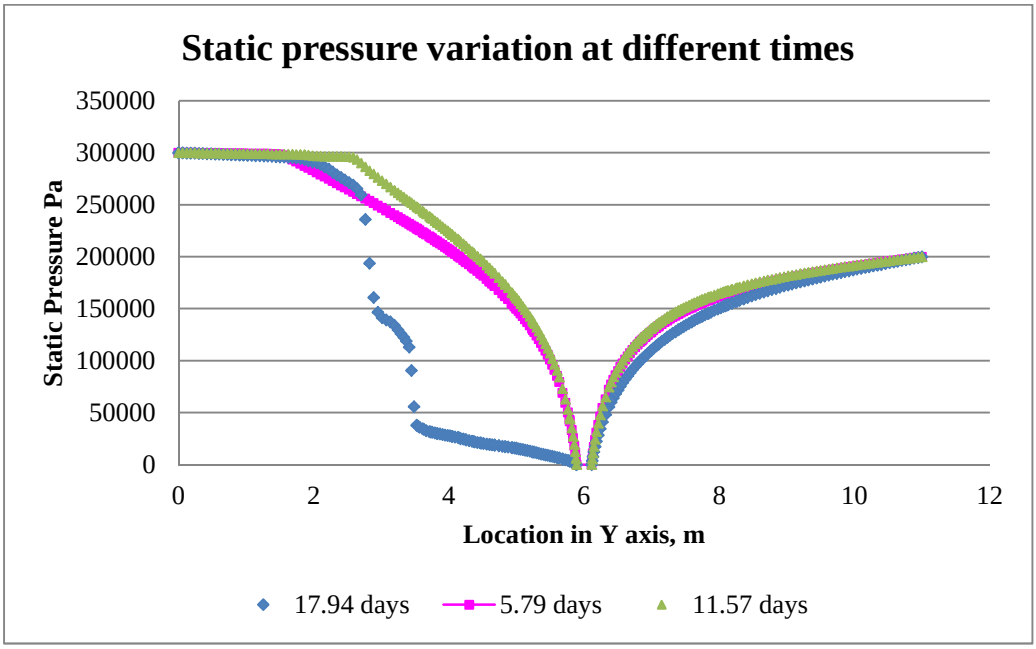


Figure 14: Static pressure variation along Y axis through the well bore

Figure 15 shows the volumetric flow rate changes with time. The volumetric flow rate of oil slightly increases with time before breakthrough. The pressure gradient increases as the water/oil interface moves towards the wellbore. The flow velocity increases with increasing pressure gradient, and hence the mass/volumetric flow to the well bore increases. After breakthrough the oil production has decreased and water production has increased and both flows exhibit considerable fluctuations. The average flow rate at the outlet before breakthrough is 0.354 $m^3$/day per 1m of the horizontal well section. Oil production from a 12.4 m section of the well is 4.4 $m^3$/day. The water flow rate fluctuates between 0 and 14 $m^3$/day after breakthrough.

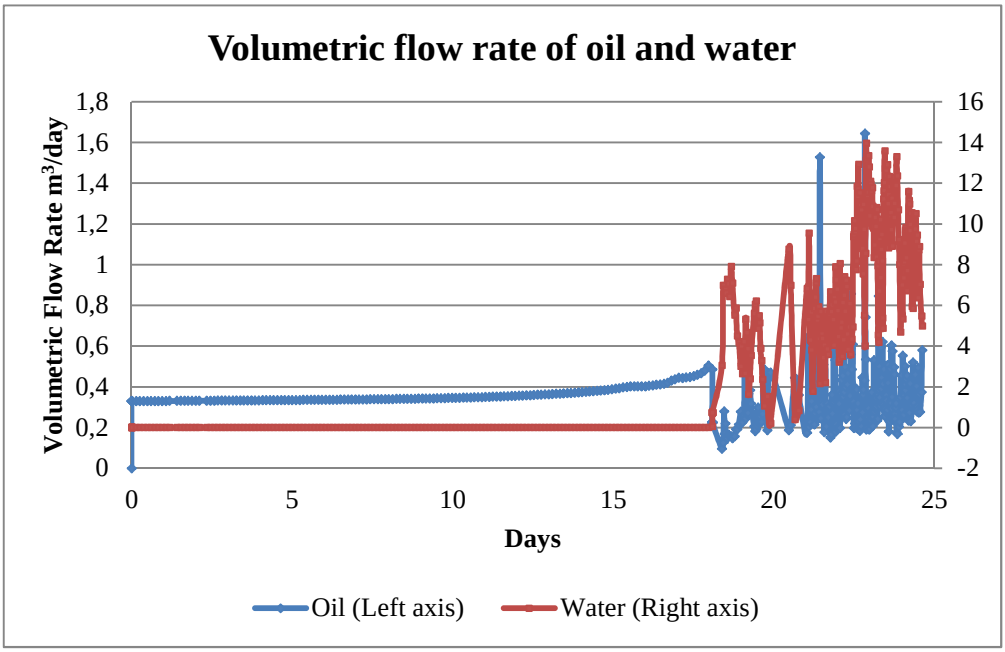


Figure 15: Volume flow as a function of time

Figure 16 presents the phase distribution after 25 days of oil production including a complex fingering behaviour. The resulting flow pattern has caused fingers of different lengths to merge, leaving islands of oil surrounded by invading water. The combined effects of spreading, tip-splitting, shielding and coalescence lead to quite complex phase distribution and unstable displacement in the porous media. When compared to Figure 13(a) which is at the time of breakthrough, several new fingers have been formed in the water oil interface away from the centre point.

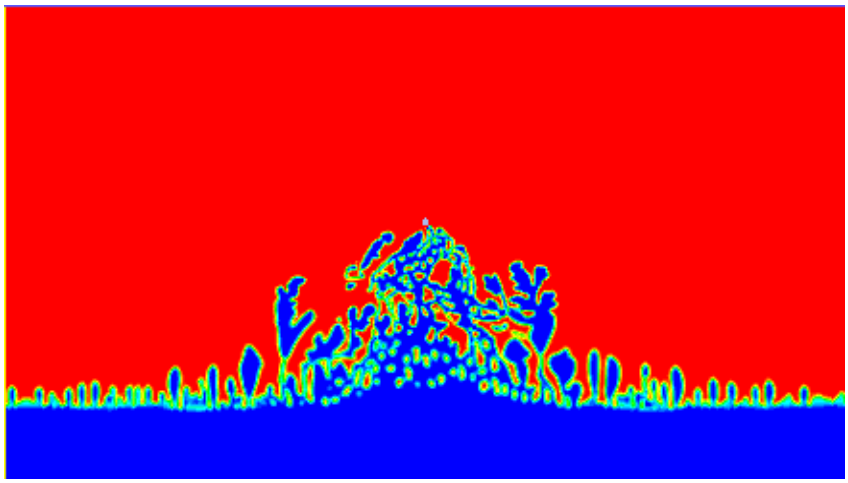

Figure 16: Contours of oil volume fraction after 25 days of oil production

# 4. Concluding remarks

Recovery of heavy viscous oil is not only associated with challenges in terms of handling and transportation, but also with problems caused by finger-like channel formation during production. Two-dimensional simulations were carried out using ANSYS/Fluent as the Computational Fluid Dynamics software. Cross section of a reservoir is simulated to study the fingering phenomenon which is instabilities that occur in the water oil contact (WOC) zone. Velocity and pressure profiles, breakthrough times and flow rates were studied. A critical velocity is calculated above which instability exists. The ANSYS VOF model is verified against experimental data found in literature. Reasonable agreement between the experimental and simulated results was obtained. According to the simulated results, oil production is highly affected by fingering behaviour, since it enables the early water breakthrough while most of the oil is still left unproduced. After the breakthrough after about 18 days, oil production is reduced while water production is increased and both flow rates exhibit considerable fluctuations. Fingering occurs due to heterogeneities in the porous media and the interaction of several forces where the viscous forces play the dominant role. The critical velocity, above which instability occurs at the water-oil interface, is $7.75 \cdot 10^{-9}$ m/s. Grid resolution and time step dependency tests were carried out to select the most suitable grid size and time step size to be used in the reservoir simulation.

**References**


1. Homsy, G.M., *Viscous fingering in porous media* Annual Review of Fluid Mechanics, 1987. **19**.
2. U.G. Araktingi and F.M. Orr, J., *Viscous Fingering in Heterogeneous Porous Media.* SPE Advanced Technology Series, 1993. **1**(1).
3. Blackwell, R.J., J.R. Rayne, and W.M. Terry, *Factors Influencing the Efficiency of Miscible Displacement.* 1959.
4. Meurs, P.V., *The Use of Transparent Three-Dimensional Models for Studying the Mechanism of Flow Processes in Oil Reservoirs.* 1957.

5. Meurs, P.v. and C.v.d. Poel, *A Theoretical Description of Water-Drive Processes Involving Viscous Fingering*. 1958.
6. Incorporation, F., *ANSYS FLUENT 12.0 User's Guide.* 2009.
7. Incorporation, F., *Fluent 6.1 Tutorial Guide.* 2003.
8. Pavone, D., *Observations and Correlations for Immiscible Viscous-Fingering Experiments.* SPE Reservoir Engineering, 1992. **7**(2).
9. Meurs, P.v. and C.v.d. Poel, *A Theoretical Description of Water-Drive Processes Involving Viscous Fingering*. 1958.